The Folding Kinetics of the SDS-Induced Molten Globule Form of Reduced Cytochrome *c*[†]

Eefei Chen,* Vanessa Van Vranken,[‡] and David S. Kliger

Department of Chemistry and Biochemistry, University of California, Santa Cruz, California 95064

Received December 16, 2007; Revised Manuscript Received February 22, 2008

ABSTRACT: The folding of reduced cytochrome *c* (redcyt *c*) is increasingly being recognized as undergoing a mechanism that deviates from a two-state process. In previous far-UV TRORD studies of redcyt *c* folding, a rapidly forming intermediate was attributed to the appearance of a molten-globule-like (MG) state [Chen, E., Goldbeck, R. A., and Kliger, D. S. (2003) *J. Phys. Chem. A 107*, 8149–8155]. A slow folding phase (>1 ms) was identified with the formation of native (N) secondary structure from that MG form. Here, using 0.65 mM SDS to induce the MG state in oxidized cytochrome *c*, folding of redcyt *c* was triggered with fast photoreduction and probed from early microseconds to milliseconds using far-UV TRORD spectroscopy. The kinetics of the reaction are described with a time constant of 50 ± 16 ms, which corresponds to 1 ± 0.6 ms upon extrapolation of the data to zero SDS concentration. The latter folding time is about 5 times faster than the calculated GuHCl-free time constant of 5.5 ± 1.4 ms for slow-phase folding obtained in our previous study. This ratio of rates would be consistent with a scenario in which 20–30% MG that is suggested to form in the fast phase of redcyt *c* folding in GuHCl is an obligatory intermediate. The native state forms from this obligatory intermediate with an observed rate, $k_f = fk_{MG\rightarrow N}$, where *f* is the fractional population of MG and $k_{MG\rightarrow N}$ is the microscopic rate for MG → N. Calculation and comparison of the $m^{\ddagger}/m$ values show agreement within the uncertainties between the SDS (∼0.5) and GuHCl (∼0.3) based redcyt *c* folding experiments, suggesting that the two experiments report on comparable intermediates. The *m* values were obtained from far-UV CD SDS titration experiments, from which calculated thermodynamic parameters allowed estimation of the reduction potential for the MG state to be ∼155 mV (−15 kJ/mol) vs NHE which, like the reduction potential for the native state, is more favorable than that for the unfolded protein.

The many functions of proteins rely on the flexibility of their structures: for example, to bind ligands or target molecules, to translocate across biological membranes, or to transition between different conformational states (*1–7*). Cellular activities such as protein degradation by ATP-dependent proteases require that the protein unfolds in order to travel through narrow channels that run along the axes of the proteasome (*6*). Various sensory and signaling proteins undergo chromophore and domain-specific polypeptide backbone conformational changes that lead to domain/domain interactions with a partner protein for downstream signal transduction (*7*). Many intrinsically disordered proteins, being extended and flexible with little to no secondary structure, can bind to a variety of substrates or partner proteins, which results in compaction to a folded state (*4*). Thus, whereas proteins are most often discussed in terms of their native state "folded" conformation, it is clear that the unfolded and the partially unfolded structures also play crucial functional roles.

A partially unfolded structure of particular note is the molten globule (MG[1]), which is characterized by a compact state with native-like secondary structure and fluctuating tertiary structure (*8–11*). The ambiguity of the term native-like leads to a fairly large range of protein structures that are defined to be molten globule (*12–15*). With that in mind, the status of the MG as a stable intermediate in *in vitro* protein folding had been controversial for years until recently, where increasing evidence has MG becoming accepted as an on-pathway intermediate (*2, 16–20*). *In vivo*, it has been proposed that the MG species is associated with several cellular processes such as transmembrane translocation, as well as with the chaperone machinery (*21–26*). The MG and other partly folded states have also been observed to play a role in human diseases, either through aggregation or through some other mechanism (*27–36*). It is clear that the fundamental steps of protein folding, involving the unfolded (U), the native (N), and the MG and other partially folded states, are important to functional successes on the cellular level. Consequently, understanding the structure and dynamics of the transition from these states to the more rigid native

[†] Supported by National Institutes of Health Grant EB02056.

* To whom correspondence should be addressed. Phone: 831.459.4007. Fax: 831.459.2935. E-mail: chen@chemistry.ucsc.edu.

[‡] Current address: University of North Carolina, Department of Chemistry, Chapel Hill, NC 27599-3290.

[1] Abbreviations: MG, molten globule; N, native protein; U, unfolded protein; redcyt *c*, reduced cytochrome *c*; oxcyt *c*, oxidized cytochrome *c*; SDS, sodium dodecyl sulfate; GuHCl, guanidine hydrochloride; TRORD, time-resolved optical rotatory dispersion; CD, circular dichroism; MCD, magnetic circular dichroism.

10.1021/bi702452u CCC: $40.75
Published on Web 04/17/2008

conformation is critical. The engineering of de novo proteins (*37*) is predicated on the knowledge of protein folding fundamentals, making it possible to test first principles while at the same time to strive to create new proteins with defined activities.

A MG-like intermediate is suggested to play a role in the mechanism of reduced cytochrome *c* (redcyt *c*) folding (*38–46*). Although such deviation from a simple two-state mechanism has been controversial, recent studies are finding increasing evidence to support it. In far-UV time-resolved optical rotatory dispersion (TRORD) studies by this group, redcyt *c* folding in the presence of increasing concentrations of GuHCl exhibited a rapid secondary structure folding process with a correspondingly faster time constant (*45*). That paper described the fast phase (<1 ms) of redcyt *c* folding in terms of formation of a MG species and a subsequent slow phase (>1 ms) wherein that MG forms native secondary structure. That hypothesis is tested here with the study of the kinetics of secondary structure folding from MG to the native state. In general, fast kinetic studies of redcyt *c* folding are limited relative to those for oxidized cytochrome *c* (oxcyt c) and still fewer can be found specifically on folding of the redcyt *c* MG (*38–48*). Although MG is most frequently observed under conditions of low or high pH (with low to moderate ionic strength), it can also be induced with low to intermediate concentrations of guanidine hydrochloride and urea, with high temperatures, with sugars, alcohols, polyanions such as poly(vinylsulfate), membrane mimetics such as anionic lysophospholipids and anionic lipid vesicles, and *n*-alkyl sulfates (*11, 15, 49–54*). *N*-Alkyl sulfates (e.g., sodium octyl sulfate, sodium dodecyl sulfate (SDS), sodium decyl sulfate, sodium tetradecyl sulfate) are anionic surfactants that are either electrostatic or hydrophobic in nature depending on the concentration. In the presence of SDS oxcyt *c* has been shown to undergo different structural changes above and below the critical micelle concentration (CMC) (*52, 55–59*). Interaction of SDS monomers, present below the CMC (2.2 mM in 45 mM NaP) (*56*), with oxcyt *c* (pH 7) results in partial unfolding of the protein. In contrast, binding of SDS micelles (above the CMC) with oxcyt *c* (pH 7) induces recovery of secondary structure.

That oxcyt *c* unfolds in the presence of SDS monomers raised the question of how the reduced species might interact with the monomers and presented the opportunity to study folding from the MG state of redcyt *c*. Previous kinetic studies of MG folding in SDS have focused on the oxidized species (*52, 56, 57, 59–62*). Thus, the first step of this study was to determine whether redcyt *c* would be more stable in SDS than is oxcyt *c*, as observed in GuHCl (*38, 39*). That is, it has been demonstrated that the folding free energies of the two redox species are different in denaturant, with redcyt *c* being more stable. Indeed, the far-UV CD SDS titration exhibited a small window of low SDS concentrations where oxcyt *c* was more unfolded than redcyt *c*, with the largest difference induced by approximately 0.65 mM SDS. With this result, the kinetics of folding of the redcyt *c* MG to the native state, triggered by rapid photoreduction (*39–41*), were accessible to TRORD methods from the nanosecond to seconds time regime. The results of the far-UV CD SDS titration, the TRORD kinetic, as well as near-UV CD and Soret and visible region magnetic CD (MCD) experiments are presented below.

MATERIALS AND METHODS

Sample Preparation. Horse heart cyt *c* (Sigma-Aldrich, St. Louis, MO), monobasic and dibasic NaP (Thermo Fisher Scientific, Waltham, MA), SDS (MP Biomedicals, Costa Mesa, CA), sodium hydrosulfite (Fluka, Ronkonkoma, NY), and NADH (Sigma-Aldrich, St. Louis, MO) were used without further purification.

The samples for the far-UV CD SDS titration of cyt *c* were prepared from two stock solutions: 20 μM oxcyt *c* and 100 mM SDS in 50 mM NaP (pH 7). Oxcyt *c* solutions were first stirred in air to oxidize all traces of redcyt *c* before CD measurements. 100 mM SDS was added in small aliquots to obtain samples with final SDS concentrations of 0, 0.1, 0.2, 0.4, 0.5, 0.6, 0.7, 0.8, 0.9, 1, 1.2, 1.4, 1.6, and 1.8 mM. Each sample was separated into two aliquots: one was for the oxcyt *c* measurement, and the second was degassed with N_2 gas before it was placed into a N_2-purged glovebag, where it was converted to redcyt *c* by addition of sodium hydrosulfite.

Oxcyt *c* and redcyt *c* samples (20 μM) for near-UV CD and Soret and visible MCD measurements were prepared using the same method as described above for the titration experiments. For these studies, samples containing 0.65 mM SDS were measured to characterize the initial and final states of the TRORD experiments. Both the CD and MCD spectra provide information on the integrity of the heme interactions in the presence of SDS. For the MCD experiments a sample of cyt *c* (20 μM) prepared in 5.5 M GuHCl was also measured to compare the ligation state of the SDS cyt *c* samples with those of a bis-his heme coordination. UV–vis spectra (UV-2101PC, Shimadzu, Columbia, MD) of the oxidized and reduced samples were collected before the CD and MCD measurements. A second spectrum was obtained for the redcyt *c* sample after each CD/MCD measurement to ensure that the solution had not reoxidized. The concentration of the GuHCl in the cyt *c* solutions was determined by refractive index measurements on a refractometer (ABBE-3L, Milton Roy).

For TRORD experiments, oxcyt *c* solutions ($\sim$20 μM) were stirred in air to oxidize trace redcyt *c*. At the same time, solid SDS was placed into a N_2-purged glovebag and after 15 min enough deoxygenated NaP (50 mM) was added to prepare a 100 mM solution. Once the oxcyt *c* solution was deoxygenated with N_2 gas, it was placed into the glovebag, where enough 100 mM SDS was added to give a final concentration of 0.65 mM SDS. In the time allotted for equilibration of the oxcyt *c*-SDS solution, solid NADH was placed into the glovebag and allowed to deoxygenate. The oxcyt *c*-SDS solution was then added to the deoxygenated solid for a final NADH concentration of 500 μM. UV–vis measurements were obtained before and after addition of SDS and after addition of NADH. Upon addition of SDS the wavelength maximum of the oxcyt *c* Soret band (409 nm) blue-shifts to 407 nm and the band increases in intensity by a factor of about 1.2. These markers were used to check that the appropriate amount of SDS (0.65 mM) had been added. The 340 nm absorbance band was monitored to determine the concentration of NADH. The addition of NADH for the kinetic experiments was not expected to change the CMC for SDS. This was confirmed by equilibrium CD measurements, where in the presence of NADH

the changes in the secondary structure for the oxidized and reduced proteins in 0.65 mM SDS are the same as without NADH.

CD and MCD Experiments. Far-UV data for the SDS titration and near-UV data were measured on a CD spectrophotometer (JASCO 720, Easton, MD, and Aviv 60DS, Lakewood, NJ) using 2 mm and 10 mm path length quartz cuvettes, respectively. The data were measured every 1 nm with a 1 nm bandwidth in the 190–300 nm and the 240–340 nm wavelength regions. Measurements used an integration time of 8 and 4 s per step, respectively. The far-UV data for the SDS titration comprises a total of 8 sets of scans, whereas 11 sets of data were averaged in the near-UV region, for each sample.

MCD measurements were collected on a CD spectrophotometer (AVIV model 60DS, Lakewood, NJ) with a 0.64 T PM-2 permanent magnet (JASCO Inc., Easton, MD). The 5 mm path length sample quartz cuvette was positioned between the two poles of the magnet. For the two different orientations of the magnetic field, antiparallel and parallel to the propagation direction of the light beam, data were collected for each sample. These data were collected every 1 nm from 350 to 650 nm with an integration time of 2 s and a 1 nm bandwidth. The data shown here represent an average of 8 experiments for each sample.

TRORD Experiments. 355 nm pulses (13–15 mJ, 7 ns, fwhm) from a Quanta Ray DCR-1 Nd:YAG laser were used to rapidly photoreduce oxcyt *c* for subsequent protein folding. The time-dependent evolution of the protein conformational changes was followed with ORD measurements. The TRORD apparatus has been described in detail elsewhere (*63*) and will only be discussed briefly here. The probe source of the TRORD apparatus was a xenon flash lamp which, initially unpolarized, was directed to a MgF_2 polarizer. The beam diameter of the linearly polarized light was then focused from ca. 6 mm to ca. 300 μm with a UV-enhanced aluminum spherical mirror (F2, Edmund Optics, Inc., Barrington, NJ). The sample cell was placed at the focus of the probe beam where it overlapped with the 1–2 mm photoexcitation beam. The flash lamp beam passed through the sample perpendicularly to the face of the cell windows and was oriented ca. 15° relative to the photoexcitation beam. A second UV-enhanced aluminum spherical mirror was used to collect the probe beam, which was then sent to a second MgF_2 polarizer, whose polarization axis was oriented perpendicularly to that of the first polarizer. The probe beam was then focused onto the slit of a spectrograph with a 600 grooves/mm grating (200 nm blaze) and detected by a multichannel CCD detector (iStar, Andor Technology, South Windsor, CT). ORD measurements involved collecting probe beam intensities when the first polarizer was rotated off the cross position (90°) of the two polarizers by $+\beta$ and then $-\beta$, with $\beta = 1.87°$ in this study. The difference between the $+\beta$ and $-\beta$ intensities divided by their sum is the ORD signal.

TRORD measurements were obtained at 2, 3, 7, 11, 50, 100 and 500 μs, 5, 10, 50, and 100 ms after initiation of redcyt *c* folding. ORD data were also collected for the pretrigger oxcyt *c* and the sodium hydrosulfite-reduced cyt *c* that was prepared at the end of the time-resolved experiments. Approximately 512–636 averages were collected for the time-resolved data, and 3440 and 768 averages were obtained for the equilibrium oxidized and reduced cyt *c* signals, respectively. Many more averages were acquired for the oxcyt *c* species because a pretrigger signal was measured before each time-resolved signal. This method of measurement was used to monitor the integrity of the solution throughout the experiment. Time-resolved measurements were collected with a repetition rate of 0.5 Hz. The sample was flowed only between laser pulses, at a rate of ~5 μL/s. This rate was determined to move all the irradiated solution out of the laser beam footprint. Sample was moved to a 2 mm path length quartz flow cell with a peristaltic pump that was placed in a N_2-purged glovebag, which also contained the deoxygenated oxcyt *c* stock solution. The postirradiated sample was exposed to air, which regenerated the oxcyt *c* for further TRORD experiments. UV–vis spectra were used to determine how much redcyt *c*, if any, remained in the oxcyt *c* solution after regeneration. Typically, the samples either were not reused or were reused only once. The sample was maintained at a temperature of 25 °C, and the temperature at the sample was checked periodically throughout the experiment with an infrared temperature probe (80T-IR, Fluke Corporation, Everett, WA).

Data Analysis. The values for the titration curve were obtained from multiwavelength CD measurements by averaging the spectrum over the wavelength range of 219–226 nm. MCD spectra were obtained from the difference of the signals obtained in the parallel and antiparallel magnetic field configurations divided by 2. The TRORD data were analyzed using difference data calculated by subtracting the pretrigger signal from the time-resolved signals. The ORD signals were offset to zero from 275 to 280 nm. Subsequently, a kinetic trace was obtained by averaging the ORD signals over the 228 to 236 nm wavelength range. The algorithms for the exponential fitting analyses were written in the mathematical software package, Matlab (The MathWorks, Inc., South Natick, MA).

The reported error bars for the far-UV CD data are the calculated standard deviations of the CD signal mean value at 222 nm, whereas those for the near-UV CD and visible MCD spectra of the redcyt *c* data are the calculated standard deviations of the CD signal mean value at 264 and 552 nm, respectively. The value at 264 nm was obtained by averaging the CD spectral data from 262 to 266 nm, the value at 552 nm was determined by averaging from 547 to 557 nm, and that for 222 nm was obtained by averaging around 217 to 227 nm.

RESULTS

The results of the SDS titration of 20 μM cyt *c* (Figure 1) showed different responses of the oxidized and reduced states to the detergent. Oxcyt *c* responds to low concentrations of SDS (<2 mM), showing a steady decrease in the magnitude of the CD signal at 222 nm from as little as 0.1 mM up to 0.6 mM. In contrast, the redcyt *c* CD signal responds quite differently, remaining relatively unperturbed until 0.6–0.7 mM SDS. After this SDS concentration the CD signal decreases in magnitude until about 1.2 mM SDS, after which it reaches approximately the same signal intensity as that for oxcyt *c*. The partly unfolded oxcyt *c* and redcyt *c* species stabilized by the presence of low SDS concentrations have about 30% less secondary structure content than the respective native species. These results show a window of SDS

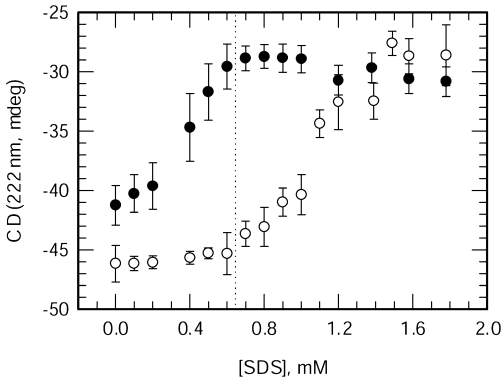

FIGURE 1: CD-detected SDS titration curves for 20 μM oxcyt *c* and redcyt *c*. Redcyt *c* (open circles) is more stable toward SDS than oxcyt *c* (black circles), as the CD signal at 222 nm for redcyt *c* does not begin to change significantly until after about 0.7 mM SDS. In contrast, the CD signal for oxcyt *c* already shows a decrease in magnitude at the lowest concentration of SDS (0.1 mM) measured. An intermediate species, having about 30% less secondary structure than native oxcyt *c* and redcyt *c*, is formed after 0.5 and 1.2 mM SDS, respectively.

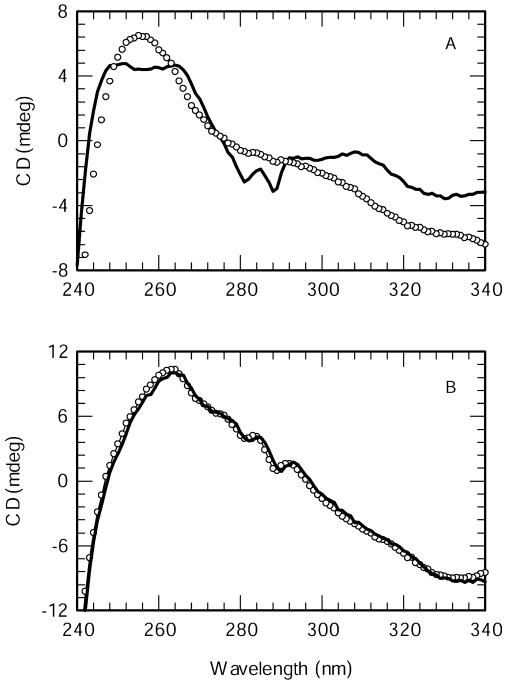

FIGURE 2: Near-UV CD spectra of 20 μM cyt *c* in 0.65 mM SDS. The near-UV CD spectra for oxcyt *c* (A) and redcyt *c* (B) in 50 mM NaP (black line) are compared with those measured in 0.65 mM SDS (open circles). Addition of 0.65 mM SDS to redcyt *c* does not appear to affect the native tertiary interactions of the protein, whereas for oxcyt *c* the near-UV CD spectra show sharpening and narrowing of the 260 nm band (heme) and disappearance of the 282 and 290 nm bands (Trp59).

concentrations where the secondary structure of oxcyt *c* is partly unfolded and that for redcyt *c* is natively folded. By using the electron-transfer trigger (*39–41*) it is possible to initiate folding of redcyt *c* by rapid photoreduction of oxcyt *c*. Because the greatest difference in the CD signal is observed at 0.6–0.7 mM SDS, the kinetics of redcyt *c* folding were measured in the presence of 0.65 mM SDS.

To further characterize the intermediate state of oxcyt *c* and redcyt *c* in 0.65 mM SDS, near-UV CD and visible MCD were measured. Figure 2 shows the near-UV CD spectra for oxcyt *c* (A) and redcyt *c* (B) with and without 0.65 mM SDS. The native state oxcyt *c* spectrum shows a positive heme band centered at 260 nm and two negative features at 282 and 290 nm that are characteristic of the Trp59 residue (*64, 65*). Upon addition of 0.65 mM SDS, the broad heme band increases in intensity and becomes narrower. The two negative bands disappear, indicating the appearance of non-native tertiary fluctuations around Trp59. These spectral changes are consistent with previously observed changes in the near-UV region that arise from addition of GuHCl and in the acid-induced MG form (*9, 66, 67*). In contrast, for redcyt *c* those two negative bands remain intact in the presence of SDS. The slight difference between the two spectra in Figure 2B is considered to be insignificant based on the standard deviation calculated for the CD spectra, suggesting that in the presence of 0.65 mM SDS the environment of the Trp59 residue in redcyt *c* is native.

MCD spectra from 450 to 560 nm, a region that is sensitive to the heme ligation state (*68, 69*), were measured to probe the nature of the heme axial coordination for oxcyt *c* in 0.65 mM SDS. In the presence of denaturants such as GuHCl and urea, it has been shown that the native Met80 ligand competes largely with non-native residues such as His and Lys for the sixth axial position (*70–75*). Consequently, to identify the heme coordination for oxcyt *c* in 0.65 mM SDS its MCD spectrum was compared to that for native oxcyt *c* at pH 7 in NaP (His18-Fe-Met) (Figure 3A) and to oxcyt *c* in 5.5 M GuHCl, pH 7 (His18-Fe-His) (Figure 3B). The MCD spectral differences in Figures 3A and 3B indicate that the His18-Fe-His heme coordination more closely describes the ligation state for oxcyt *c* in SDS than the His18-Fe-Met axial ligation. Figure 3C shows an overlay of the MCD spectra obtained by a linear combination of the MCD spectrum of oxcyt *c* in 5.5 M GuHCl and the MCD spectrum of native oxcyt *c* (His18-Fe-Met) with the MCD spectrum of oxcyt *c* in 0.65 mM SDS. The good overlay of the two spectra suggests that in 0.65 mM SDS oxcyt *c* has ~85% His18-Fe-His and ~15% His18-Fe-Met heme coordinations. For redcyt *c* in 0.65 mM SDS the Soret and visible MCD features differ from the native redcyt *c* spectrum by only a slight decrease in the intensity of the bands (Figure 3D). Although the change in intensity is small (~6%), it is significant based on the calculation of the uncertainty (1%) of the MCD value averaged from 547 to 557 nm. The MCD spectrum for redcyt *c* in 0.65 mM SDS clearly does not have a His18-Fe-His heme coordination because in the presence of 6 M GuHCl the MCD spectrum for redcyt *c* is red-shifted by approximately 5 nm and is about 50% less intense than that for the native protein (*73*).

The results of the near-UV CD and MCD measurements indicate that in 0.65 mM SDS oxcyt *c* has fluctuating tertiary structure. The intermediate species induced by 0.65 mM SDS contains about 70% of the native oxcyt *c* secondary structure. These structural features, near-native secondary structure and non-native tertiary contacts, describe a MG-like oxcyt *c* intermediate. In contrast, at the same concentration of SDS, redcyt *c* exhibits native secondary structure and near-native tertiary contacts. As was true for the far-UV CD above, Figure 4A demonstrates that in 0.65 mM SDS the ORD signal for 20 μM oxcyt *c* is also smaller in magnitude relative to redcyt *c*. Thus, rapid photoreduction of the MG-like oxcyt *c* yields an immediate, structurally equivalent redcyt *c* photoproduct. However, at this concentration of SDS redcyt

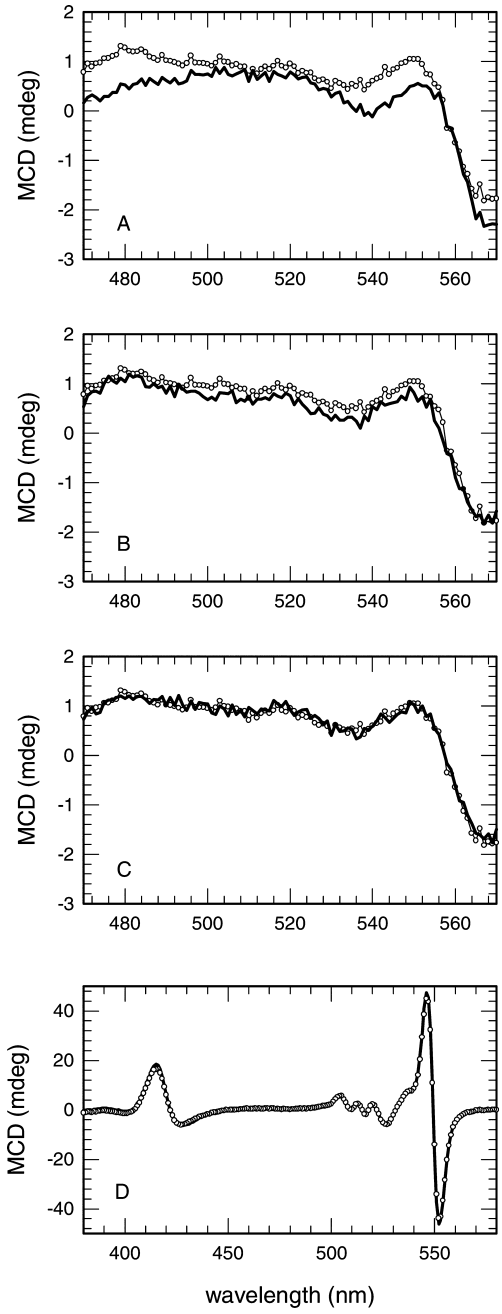

FIGURE 3: Equilibrium MCD spectra of 20 μM oxcyt *c* in 0.65 mM SDS, in 50 mM NaP and in 5.5 M GuHCl. (A) When the visible MCD spectrum of oxcyt *c* in 0.65 mM SDS, pH 7, (thin line, open circles) is overlaid with the spectrum for native oxcyt *c* in NaP at pH 7 (solid black line), it is clear that the heme coordination for the former is not the native His18-Fe-Met80 ligation. (B) This panel shows that the MCD spectrum for oxcyt *c* in 0.65 mM SDS (thin line, open circles) more closely resembles that for oxcyt *c* in 5.5 M GuHCl, pH 7 (solid black line). The MCD spectrum for oxcyt *c* in SDS (thin line, open circles) overlays well with the spectrum obtained from a linear combination of the oxcyt *c* MCD spectra measured in NaP (15%) and in 5.5 M GuHCl (85%) (solid black line) (C). (D) In this panel, the MCD spectrum for redcyt *c* in 0.65 mM SDS (thin line, open circles) is overlaid with that for redcyt *c* in NaP (solid black line).

c favors the native secondary structure fold and, thus, the protein undergoes secondary structure folding from the MG-like conformation. Figure 4B shows the difference kinetic trace obtained from the multichannel difference TRORD data (not shown) measured at 2, 3, 7, 11, 50, 100, and 500 μs, 5, 10, 50, and 100 ms. The ORD signal shows no significant

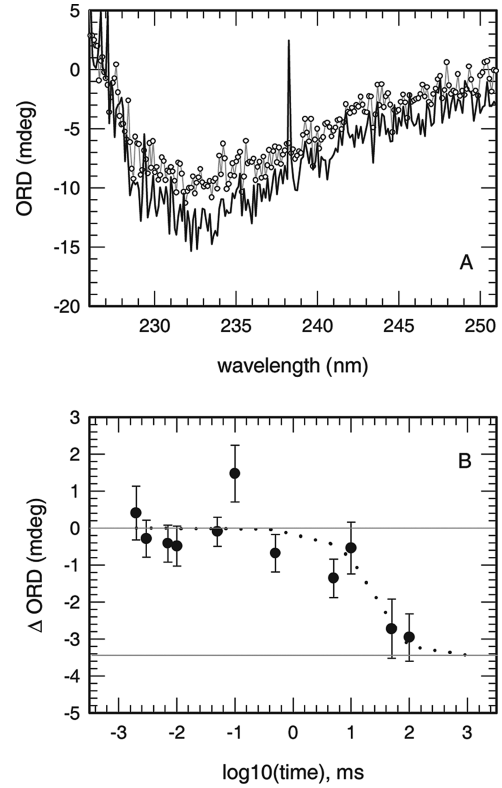

FIGURE 4: TRORD results for redcyt *c* folding in 0.65 mM SDS. (A) The ORD signals indicate that 20 μM oxcyt *c* in 0.65 mM SDS (gray line, open circles) is partly unfolded by about 30% relative to redcyt *c* in 0.65 mM SDS (solid black line), which is fully folded. (B) In this panel, the difference far-UV TRORD data (black circles), measured upon photoreduction of oxcyt *c*, show no changes in the ORD signal between 2 and approximately 500 μs, after which the signal increases with a time constant of about 50 $\pm$ 16 ms. The fit of the data (dashed line) is shown along with the TRORD data. In the TRORD data, the increase in ORD signal magnitude is $\sim$30% upon formation of redcyt *c* from oxcyt *c*.

change from 2 μs until after about 1 ms, where it begins to grow until it reaches completion. These data are best fit to a single exponential decay with a time constant of $\sim$50 $\pm$ 16 ms. The increase in the magnitude of the ORD signal is correlated with the changes in secondary structure as the immediate, partly unfolded redcyt *c* photoproduct folds to its native secondary structure configuration.

DISCUSSION

The interaction of oxcyt *c* with SDS monomers has previously demonstrated a small loss of secondary structure and a significant loss of tertiary contacts (*52, 55–59*). According to Oellerich et al. (*57*) and Das et al. (*52*), the far-UV CD spectra of oxcyt *c* as a function of SDS concentration show a decrease in intensity (by $\sim$25%) that reaches a plateau by about 0.9 mM. The results of near-UV CD and Trp59 fluorescence studies indicate that the tertiary contacts found in the native oxcyt *c* protein are disrupted by 0.8 to 0.9 mM SDS. Such spectral descriptions are hallmarks of a MG, and thus, with SDS monomers it is possible to trap oxcyt *c* in such an intermediate state. The first goal of this study was to investigate the secondary structure unfolding stabilities of the reduced state of cyt *c* toward SDS, which was not previously examined, and to compare the SDS titration curve with that for oxcyt *c*. If the two proteins

exhibited different unfolding stabilities, the second goal was to study the secondary structure kinetics of redcyt *c* folding, triggered by rapid electron transfer, from the MG state using far-UV TRORD detection. The initial (oxcyt *c*) and final (redcyt *c*) samples were characterized using near-UV CD and visible MCD spectroscopy: the third goal. And finally, the results of these kinetics studies are compared to previously reported (by this group) far-UV TRORD experiments of redcyt *c* folding to determine whether the slow phase of those studies can be attributed to folding of a MG intermediate.

Spectral Characterization of Oxcyt c and Redcyt c. The spectral properties of redcyt *c* in the presence of SDS were determined using CD and MCD methods in order to understand the final protein conformation expected in the kinetics experiment. Although previous studies have characterized the changes in oxcyt *c* induced by low concentrations of SDS, oxcyt *c* was examined again to compare the starting material here to those described in earlier reports. The tertiary contact between the protein and the heme group was also examined from the point of view of the heme axial coordination. The results of near-UV CD measurements confirm that for oxcyt *c* native tertiary contacts have been compromised by the presence of SDS (0.65 mM). A comparison of MCD spectra indicates that, in 0.65 mM SDS, oxcyt *c* has largely His18-Fe-His heme ligation, with a small percentage of His18-Fe-Met heme coordination (15%). Previous absorption and resonance Raman studies indicate that by 2 mM SDS, the heme coordination in oxcyt *c* is 100% His18-Fe-His (*52, 57*), but at 0.7 mM SDS (50 mM NaP, pH 7) there is about 65:35 contribution of the respective His18-Fe-His and His18-Fe-Met axial ligations to a 15 μM oxcyt *c* solution (*57*). The discrepancy in the percentage of His18-Fe-His heme coordination may be due to differences in the experimental conditions and does not detract from the main point that the interaction of oxcyt *c* with SDS perturbs the native heme ligation.

The far-UV CD SDS titration of redcyt *c* demonstrates that redcyt *c* has greater stability toward the denaturant than oxcyt *c*. The near-UV CD data for redcyt *c* indicate that the Trp59 interaction with the heme group is not disrupted by 0.65 mM SDS. Although the slight decrease in intensity around the 260 nm heme near-UV CD band is not considered to be significant, there is a decrease in intensity detected in the MCD spectra. These results suggest that whereas redcyt *c* in the presence of SDS maintains its native tertiary interactions, such interactions might be more relaxed than those in the native conformation.

Thermodynamic Parameters of Oxcyt c and c Redcyt Folding. Assuming a two-state transition and using the native and MG states as the end points to calculate the fraction of protein that is unfolded as a function of SDS, the free energies of folding between N and MG were calculated using the equation $\Delta G_f = -RT \ln K_f$. A linear plot of ΔG_f versus [SDS] allowed extrapolation of the free energy of folding in the absence of SDS (ΔG_f°). The *m* value, which is proportional to the exposure of the protein surface to solvent during formation of the unfolded (or transition) state, was calculated from the equation $\Delta G_f = \Delta G_f^\circ + m[\mathrm{SDS}]$ (*76–79*). The $\Delta G_f^\circ{}_{(MG\rightarrow N)}$ and *m* values obtained from the two-state fit of the far-UV CD data (Figure 1) are respectively −10 kJ/mol and 28,500 kJ mol^{-1} M^{-1} for oxcyt *c* and −17 kJ/mol and 16,700 kJ mol^{-1} M^{-1} for redcyt *c* (summarized in Table 1). The *m* values reflect the strength of the denaturant: the C_m values for oxcyt *c* and redcyt *c* in SDS are respectively about 0.4 and 1 mM, which is considerably less than the C_m values measured in GuHCl (2.8 and ∼5 M) (*40, 73*). Thus, the much smaller *m* values of 14.3 kJ/mol (oxidized) and 13.8 kJ/mol (reduced) for folding from U to N in GuHCl are not unusual. Between oxcyt *c* and redcyt *c* in SDS, the *m* values describe differences in protein unfolding that may arise from the anionic nature of SDS and its interaction with the differently charged cyt *c* proteins.

Table 1: Thermodynamic and Kinetic Parameters for the Slow Phase of Cytochrome *c* Folding

reaction	denaturant	ΔG_f° (kJ mol^{-1})	*m* (kJ mol^{-1} M^{-1})	$m^\ddagger$ (kJ mol^{-1} M^{-1})	$m^\ddagger/m$
oxidized					
U → N ([a])	GuHCl	−40 ± 1	14.3 ± 4		
U → N ([b])	GuHCl	−31 ± 0.3	13 ± 1.3		
MG → N	SDS	−10 ± 1	28,500 ± 5000		
reduced					
U → N ([a])	GuHCl	−74 ± 3	13.8 ± 4	5.6 ± 0.5	0.4
U → N ([b])	GuHCl	−65 ± 7	11 ± 1	3 ± 1	0.3
MG → N	SDS	−17 ± 1	16,700 ± 1000	8300 ± 4000	0.5

[a] Thermodynamic parameters (22 °C) from Mines et al. (*40*). The $m^\ddagger$ value represents the slow phase of folding from the initially unfolded state. The $m^\ddagger/m$ value is similar to that reported by Pascher (*43*). [b] These thermodynamic parameters are based on polarization methods (20 °C), and kinetic parameters are from TRORD spectroscopy (25 °C) (*45, 73*). The $m^\ddagger$ values were calculated from the kinetic parameters for the slow phase of folding from the initially unfolded state.

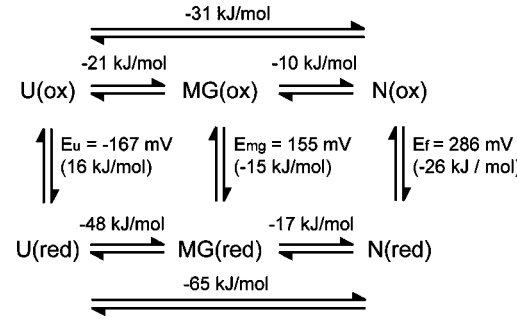

FIGURE 5: Thermodynamic cycle for oxcyt *c*, redcyt *c* and MG cyt *c* folding. The free energy values for the reduction of native (−26 kJ/mol) and unfolded (16 kJ/mol) oxcyt *c* were calculated from the reduction potentials reported previously by Bixler et al. (E_u = –167 mV vs NHE and E_f = 286 mV vs NHE) (*82*). From the unfolding curves shown in Figure 1 $\Delta G_f^\circ{}_{(MG\rightarrow N)}$ was calculated to be −10 kJ/mol for oxcyt *c* and −17 kJ/mol for redcyt *c*. Using the $\Delta G_f^\circ{}_{(U\rightarrow N)}$ values for oxcyt *c* (−31 kJ/mol) and redcyt *c* (−65 kJ/mol) (*73*), $\Delta G_f^\circ{}_{(U\rightarrow MG)}$ values were calculated to be −21 and −48 kJ/mol, respectively. The estimated free energy (−15 kJ/mol) and reduction potential (155 mV) values for the MG state refer to the full cell reaction with NHE.

A breakdown of the ΔG_f° values is shown with the thermodynamic cycle in Figure 5. The difference between the free energies of oxcyt *c* folding from U to N ($\Delta G_f^\circ{}_{(U\rightarrow N),ox}$ ∼ −31 kJ/mol) (*73, 80*) and from MG to N ($\Delta G_f^\circ{}_{(MG\rightarrow N),ox}$ ∼ −10 kJ/mol) shows that the driving force for formation of MG from U ($\Delta G_f^\circ{}_{(U\rightarrow MG),ox}$ ∼ −21 kJ/mol) is greater than that for folding of MG to N. The same is true for redcyt *c*. That is, the driving force for the U → MG process ($\Delta G_f^\circ{}_{(U\rightarrow MG),red}$ ∼ −48 kJ/mol) is greater than that for the MG → N step ($\Delta G_f^\circ{}_{(MG\rightarrow N),red}$ ∼ −17 kJ/mol), where $\Delta G_f^\circ{}_{(U\rightarrow N),red}$ ∼ −65 kJ/mol (*73*). These values are not surprising given the nature of the MG state: the formation of the MG involves polypeptide collapse, whereas the final state is achieved after search of the MG for native contacts.

Compared to previously reported data for oxcyt *c*, the calculated value for $\Delta G_f^{\circ}{}_{(U\rightarrow MG),ox}$ of −21 kJ/mol is consistent with that measured for the acid-induced MG state (−17.3 kJ/mol (*81*)). The −10 kJ/mol ($\Delta G_f^{\circ}{}_{(MG\rightarrow N),ox}$) measured in these experiments is similar to the value of −15 to −19.3 kJ/mol measured for oxcyt c (MG to N) in the presence of SDS (*52*). The greater stability for the reduced form versus the oxidized form of MG is consistent with the greater stability of the overall U to N redcyt *c* folding. That is, redcyt *c* is about twice as stable as oxcyt *c* in both U → MG and MG → N. Although the reduction potentials for the unfolded and folded (−100 to −200 mV vs NHE and ∼270 mV vs NHE, respectively) states of the oxcyt *c* have been reported by several studies (*39, 40, 82–85*), the values used in the thermodynamic cycle are those reported by Bixler et al. (E_u = −167 mV and E_f = 286 mV vs NHE) (*82*). The corresponding calculated free energies of 16 and −26 kJ/mol, respectively, refer to the full cell reactions with the NHE and are used to obtain an estimated reduction potential for the MG state of ∼155 mV (−15 kJ/mol) vs NHE. This MG reduction potential, like the reduction potential for the native state, is more favorable than that for the unfolded protein.

Kinetics of Molten Globule Redcyt c Folding. The fast kinetics (that is, kinetics within the burst phase of conventional stopped-flow experiments) of redcyt *c* folding have been probed previously from the largely unfolded to the native (or nearly native) state. In those studies, folding was triggered using ligand photolysis and rapid electron transfer initiation methods (*38–48*). The success of the electron-transfer trigger method relies on the difference in folding free energies for oxcyt *c* and redcyt *c* in the presence of GuHCl. For example, in the presence of 3 to 5 M GuHCl oxcyt *c* is largely unfolded whereas redcyt *c* is natively folded. Consequently, with an electron transfer photoevent, it is possible to rapidly reduce the initially unfolded oxcyt *c* sample and trigger redcyt *c* to fold. Protein folding can then be monitored from hundreds of nanoseconds to seconds.

The results of these far-UV TRORD studies show that secondary structure folding from the redcyt *c* MG to the native state proceeds with a time constant of 50 ± 16 ms. In general it is complicated to make a direct comparison of equilibrium and kinetic intermediates because they often cannot be observed under the same experimental conditions. For example, the acid-induced MG is obtained at pH 2 in the presence of salt, but folding of that A-state cyt *c* requires dilution into buffer near neutral pH. The same is true for dilution of SDS when using stopped-flow methods to probe folding of the SDS-induced MG state. Using the electron-transfer trigger method to initiate folding of the MG state has the advantage that folding of the observed equilibrium intermediate occurs under the same experimental conditions.

The kinetics of oxcyt *c* MG folding (pH 7) in the presence of SDS monomers have been probed with fluorescence spectroscopy and initiated by stopped-flow dilution (*52, 61*). Although two processes have been observed with time constants greater than 1 s in these studies, Das et al. (*52*) also report a time constant of 8 ms that was assigned to dissociation of His26 because of its similarity to the results published by Colon et al. (*72*). Assuming that the two redox species of cyt *c* have similar kinetics of folding from the MG state, then the combination of the results of oxcyt *c* and redcyt *c* folding suggest that dissociation of the non-native His18-Fe-His (8 ms) is followed by secondary structure formation to the native conformation within 50 ms. Tertiary rearrangements, polypeptide chain reorganization and proline isomerization (>1 s), that follow would not be observed in the results of these studies that focus on the dynamics of the secondary structure.

One of the underlying motivations for studying the folding of the MG intermediate to the native state was to determine whether the kinetics of the folding reaction for redcyt *c* in the presence of GuHCl (pH 7), triggered by an electron-transfer event, proceeded through a MG intermediate (i.e., U → MG → N) (*45*). The results of those studies showed two phases, where the fast phase (<1 ms) was considered to reflect formation of a MG intermediate and the slow phase (>1 ms) was correlated to the formation of the native state from MG. To compare the kinetics of the MG → N redcyt *c* processes from the GuHCl and the SDS experiments, it is necessary to extrapolate the data to zero denaturant. For the slow phase (MG → N) of the U → MG → N redcyt *c* folding reaction in GuHCl such an extrapolation gives a time constant of 5.5 ± 1.4 ms. Far-UV TRORD experiments measured at 0.5 mM SDS were paired with the data acquired at 0.65 mM SDS to give a folding time constant of about 1 ± 0.6 ms in 0 mM SDS. Although the data for 0.5 mM SDS are preliminary (τ = 21 ± 13 ms), the time constant in zero denaturant would correspond to about a 20% population of MG, given the calculated GuHCl-free time constant of 5.5 ms for slow phase folding and the assumption that MG is an obligatory intermediate for the pathway U ↔ MG → N. This percentage is consistent with the 20–30% MG that is suggested to form in the fast phase of redcyt *c* folding in GuHCl (U ↔ MG → N) (*45*), assuming that there is a fast equilibrium between the U and MG states. These results suggest that the transient observed in redcyt *c* folding (in GuHCl) is indeed a productive MG intermediate. The native state forms from this obligatory MG intermediate with an observed rate, $k_f = fk_{MG\rightarrow N}$ where *f* is the fractional population of MG and $k_{MG\rightarrow N}$ is the microscopic rate for MG → N.

In studies of electron-transfer triggered folding of redcyt *c* measured in 2.3 to 4.6 M GuHCl (pH 7, 40 °C) using absorption spectroscopy, Pascher et al. also interpreted their results in terms of a U → I → N mechanism (*39*). But, the slow phase (I → N) data are difficult to compare because they were either measured at 40 °C (τ ∼ 500 μs in 0.7 M GuHCl/τ ∼100 μs in 0 M GuHCl) or extrapolated to 10 °C in 0.7 M GuHCl (τ = 2 ms). At 22.5 °C, Mines et al. (*40*) focused on that slow phase of folding and reported similar extrapolated values for folding in zero denaturant to those by Pascher et al. (*39*). Generally, the measured time constants are faster than those reported for the slow phase (MG → N) of the far-UV TRORD studies. At least two factors may contribute to these differences in the far-UV TRORD and the absorption data. First, I and MG may not be the same states given the use of two different triggers to initiate and probe folding on different time scales in the absorption data. Second, in the event that the processes probed are the same, different kinetic data may still be reported depending on which part of the protein is being monitored. Such factors may also explain the much faster reaction kinetics (τ ∼ 12 μs) triggered by a CO-photolysis event that was reported for their M−CO intermediate (compact, highly structured with native-like helix and non-native tertiary structure and

heme coordination) based on heme optical absorption data by Pabit et al. (*46*).

The results of the comparison of the SDS and GuHCl far-UV TRORD data provide some support for the idea that folding of redcyt *c* initiated by fast photoreduction proceeds through a MG intermediate. This redcyt *c* intermediate is formed as fast as 400 ns (4 M GuHCl) and corresponds to formation of 20% secondary structure by the end of the fast phase (*45*). In ref *45* it was suggested that only 20% of the unfolded protein molecules are poised for rapid polypeptide collapse to the compact MG intermediate. The trend observed for the time constant of redcyt *c* folding with increasing concentrations of GuHCl is that the risetime of the secondary structure formation slows considerably with less denaturant. That is, formation of secondary structure in the fast phase occurs with a time constant of about 12 μs at 2.7 M GuHCl and within 400 ns at 4 M GuHCl. How would or could a MG intermediate form on such a fast time scale? The appearance of MG in this fast folding phase is consistent with an intermediate species, having near-native secondary structure and fluctuating tertiary interactions, being populated with increasing denaturant in the equilibrium unfolding of redcyt *c* (*73*). The results of this study and the ones mentioned above provide increasing evidence for folding of redcyt *c* via an intermediate state. In an additional time-resolved fluorescence and absorption study of redcyt *c* folding triggered by photoreduction, Pascher observed nonlinearity of the rate constant for redcyt *c* folding from 1 ms to 10 s (phase 4) as a function of GuHCl (1.63–4.9 M) (*43*). It was proposed that the nonlinearity reflected a mechanism that was more complex than simple two-state folding. When the data from the region where the nonlinearity appears is eliminated, the kinetics resembled the data from the earlier work by Pascher et al. on redcyt *c* folding (*39*). However, when the data by Pascher are compared only in the denaturant concentration range that was used in the far-UV TRORD studies (*45*), the data are more consistent with the TRORD results, with an extrapolated time constant of folding in zero GuHCl of 1.2 ms. The different kinetic results suggest the need for caution when trying to compare data measured in different denaturant concentration ranges and with different optical probes.

With that in mind, the values of $m^{\ddagger}$ and $m^{\ddagger}/m$ (*76, 86*) were calculated to compare the position of the intermediate along the reaction pathway for SDS- and GuHCl-induced redcyt *c* folding observed with TRORD methods. The values for $m^{\ddagger}$ were determined with the equation ($\Delta G_f^{\ddagger} = \Delta G_f^{\circ\ddagger} + m^{\ddagger}$[SDS]) analogous to that used to calculate ΔG_f° (see above) and are summarized in Table 1, along with the values for $m^{\ddagger}/m$. The value of $m^{\ddagger}/m$ gauges the average solvent accessibility (compactness) of the transition state relative to the U and N states. For the GuHCl and the SDS TRORD studies, the values of $m^{\ddagger}/m$ (0.3 and 0.5) are consistent within the uncertainties of the measurements, suggesting that the intermediate structures from the two studies are similar. The values of $m^{\ddagger}/m$ from the TRORD data are also, within the uncertainties of the measurements, consistent with the values reported by Mines et al. and Pascher (*40, 43*). Using their rates measured only in the same concentration range and about the same temperature used in the far-UV TRORD studies (*45*), an average $m^{\ddagger}/m$ value is calculated to be about 0.35. These are rough comparisons, as the $m^{\ddagger}/m$ value for the SDS studies is a more direct measure of the MG to N process, whereas the GuHCl data follows the entire U → I (or MG) → N folding process. From the values of $m^{\ddagger}/m$, the transition state for MG → N appears to be almost halfway between the MG and N states of the redcyt *c* protein. At present, the close values of $m^{\ddagger}/m$ measured by the various studies suggest that the differences in the redcyt *c* folding rates are largely due to the differences in the detection method used to probe the same, or very similar, intermediate species (MG, I) in the U → MG → N (*45*) and U → I → N (*39, 40, 43*) folding reactions. That apparently comparable intermediates are detected in these various experiments suggests that the rate limiting step in redcyt *c* folding occurs during the slow phase. The debate of on-pathway versus off-pathway folding intermediates is ongoing for both redcyt *c* and oxcyt *c* and certainly cannot be resolved with these studies (*87–91*). However, together with the $m^{\ddagger}/m$ value comparison, the fact that the fraction of the signal formed in the fast phase of redcyt *c* folding (assigned to an MG transient) is similar to the ratio of the observed slow-phase folding rate for U → N and the rate for MG → N suggests, but does not prove, that the MG species is a productive intermediate.

CONCLUSIONS

According to the thermodynamic parameters calculated from the unfolding SDS titration curves for oxcyt *c* and redcyt *c*, the driving force for formation (U → MG) of the MG intermediate is greater than that for formation of the native protein secondary structure (MG → N). From the thermodynamic cycle, the reduction potential and corresponding free energy of the MG state are calculated to be ~155 mV (−15 kJ/mol) vs NHE. Previous studies using far-UV TRORD methods to probe the redcyt *c* folding reaction in GuHCl revealed a fast and a slow phase (*45*). Focusing on the slower phase, the kinetic results of this study with SDS provide support for the suggestion that the mechanism of redcyt *c* secondary structure folding involved formation of the native conformation from an MG intermediate species (MG → N). Using SDS to poise oxcyt *c* in the MG state, redcyt *c* was triggered to fold to its native secondary structure upon rapid photoreduction. A calculation of the folding time constant at zero SDS gives about 1 ± 0.6 ms, which is roughly consistent with the results of redcyt *c* folding (τ = 5.5 ± 1.4 ms) in the absence of GuHCl. This result provides support for MG being a productive intermediate.

The results of this study provide additional information toward the long-term goal of understanding the fundamental elements of protein folding in cytochrome *c*, as well as for proteins in general. Although there are fundamental differences between the conditions typical of *in vitro* and *in vivo* experiments, with respect to protein concentration/cellular crowding and the use of denaturant, studies increasingly suggest that the basic tenets of *in vitro* folding hold true for *in vivo* folding (*92, 93*). Thus, understanding the structure and dynamics of the unfolded and partly unfolded intermediates of proteins promises to be important to understanding both the folding of proteins and the impact of folding dynamics on cellular processes.

ACKNOWLEDGMENT

We thank Volodya Uversky and Robert Goldbeck for helpful discussions and insights.

REFERENCES

1. Wright, P. E., and Dyson, H. J. (1999) Intrinsically unstructured proteins: Re-assessing the protein structure-function paradigm. *J. Mol. Biol. 293*, 321–331.
2. Ptitsyn, O. B. (1995) Molten globule and protein folding. *Adv. Protein Chem. 47*, 83–229.
3. Uversky, V. N., Gillespie, J. R., and Fink, A. L. (2000) Why are 'natively unfolded' proteins unstructured under the physiological conditions? *Proteins: Struct., Funct., Genet. 41*, 415–427.
4. Uversky, V. N. (2002) What does it mean to be natively unfolded? *Eur. J. Biochem. 269*, 1–10.
5. Tompa, P. (2002) Intrinsically unstructured proteins. *TIBS 27* (10), 527–533.
6. Prakash, S., and Matouschek, A. (2004) Protein unfolding in the cell. *TIBS 29* (11), 593–600.
7. Cusanovich, M. A., and Meyer, T. E. (2003) Photoactive yellow protein: A prototypic PAS domain sensory protein and development of a common signaling mechanism. *Biochemistry 42*, 4759–4770.
8. Ptitsyn, O. (1995) How the molten globule became. *TIBS 20*, 376–379.
9. Dolgikh, D. A., Gilmanshin, R. I., Brazhnikov, E. V., Bychkova, V. E., Semisotnov, G. V., Venyaminov, S. Y., and Ptitsyn, O. B. (1981) α-Lactalbumin: Compact state with fluctuating tertiary structure? *FEBS Lett. 136*, 311–315.
10. Ohgushi, M., and Wada, A. (1983) 'Molten globule state': A compact form of globular proteins with mobile side-chains. *FEBS Lett. 164*, 21–24.
11. Dolgikh, D. A., Abaturov, L. V., Bolotina, I. A., Brazhnikov, E. V., Bychkova, V. E., Gilmanshin, R. I., Lebedev, Y. O., Semisotnov, G. V., Tiktopulo, E. I., and Ptitsyn, O. B. (1985) Compact state of a protein molecule with pronounced small-scale mobility: bovine α-lactalbumin. *Eur. Biophys. J. 13*, 109–121.
12. Nishii, I., Kataoka, M., Tokunaga, F., and Goto, Y. (1994) Cold denaturation of the molten globule states of apomyoglobin and a profile for protein folding. *Biochemistry 33*, 4903–4909.
13. Redfield, C., Smith, R. A. G., and Dobson, C. M. (1994) Structural characterization of a highly-ordered 'molten globule' at low pH. *Nat. Struct. Biol. 1*, 23–29.
14. Bychkova, V. E., Dujsekina, A. E., Klenin, S. I., Tiktopulo, E. I., Uversky, V. N., and Ptitsyn, O. B. (1996) Molten globule-like state of cytochrome *c* under conditions simulating those near the membrane surface. *Biochemistry 35*, 6058–6063.
15. Moza, B., Qureshi, S. H., Islam, A., Singh, R., Anjum, F., Moosavi-Movahedi, A. A., and Ahmad, F. (2006) A unique molten globule state occurs during unfolding of cytochrome *c* by $LiClO_4$ near physiological pH and temperature: Structural and thermodynamic characterization. *Biochemistry 45*, 4695–4702.
16. Uversky, V. N., Semisotnov, G. V., Pain, R. H., and Ptitsyn, O. B. (1992) 'All-or-none' mechanism of the molten globule unfolding. *FEBS Lett. 314*, 89–92.
17. Dobson, C. M. (1994) Solid evidence for molten globules. *Curr. Biol. 4*, 636–640.
18. Uversky, V. N., and Ptitsyn, O. B. (1996) All-or-none solvent-induced transitions between native, molten globule and unfolded states in globular proteins. *Folding Des. 1*, 117–122.
19. Fink, A. L. (2001) Molten globule. *Encycl. Life Sci.* 1–6.
20. Cecconi, C., Shank, E. A., Bustamante, C., and Marqusee, S. (2005) Direct observation of the three-state folding of a single protein molecule. *Science 309*, 2057–2060.
21. Bychkova, V. E., Pain, R. H., and Ptitsyn, O. B. (1988) The 'molten globule' state is involved in the translocation of proteins across membranes? *FEBS Lett. 238* (2), 231–234.
22. Martin, J., Langer, T., Boteva, R., Schramel, A., Horwich, A. L., and Hartl, F. U. (1991) Chaperonin-mediated protein folding at the surface of groEL through a 'molten globule'-like intermediate. *Nature 352*, 36–42.
23. van der Goot, F. G., González-Mañas, J. M., Lakey, J. H., and Pattus, F. (1991) A 'molten-globule' membrane insertion intermediate of the pore-forming domain of colicin A. *Nature 354*, 408–410.
24. Bychkova, V. E., and Ptitsyn, O. B. (1993) The molten globule in vitro and in vivo. *Chemtracts—Biochem. Mol. Biol. 4*, 133–163.
25. Hartl, F. U., Hlodan, R., and Langer, T. (1994) Molecular chaperones in protein folding: The art of avoiding sticky situations. *Trends Biochem. Sci. 19*, 20–25.
26. Lu, H., Golovanov, A. P., Alcock, F., Grossmann, J. G., Allen, S., Lian, L.-Y., and Tokatlidis, K. (2004) The structural basis of the TIM10 chaperone assembly. *J. Biol. Chem. 279*, 18959–18966.
27. Rajaraman, K., Raman, B., Ramakrishna, T., and Rao, C. M. (1998) The chaperone-like α-crystallin forms a complex only with the aggregation-prone molten globule state of α-lactalbumin. *Biochem. Biophys. Res. Commun. 249*, 917–921.
28. Gillmore, J. D., and Hawkins, P. N. (1999) Amyloidosis and the respiratory tract. *Thorax 54*, 444–451.
29. Morrow, J. A., Hatters, D. M., Lu, B., Höchtl, P., Oberg, K. A., Rupp, B., and Weisgraber, K. H. (2002) Apolipoprotein E4 forms a molten globule. *J. Biol. Chem. 277*, 50380–50385.
30. Horwich, A. (2002) Protein aggregation in disease: a role for folding intermediates forming specific multimeric interactions. *J. Clin. Invest. 110*, 1221–1232.
31. Selkoe, D. J. (2003) Folding proteins in fatal ways. *Nature 426*, 900–904.
32. Almstedt, K., Lundqvist, M., Carlsson, J., Karlsson, M., Persson, B., Jonsson, B.-H., Carlsson, U., and Hammarström, P. (2004) Unfolding a folding disease: Folding, misfolding and aggregation of the marble brain syndrome-associated mutant H107Y of human carbonic anhydrase II. *J. Mol. Biol. 342*, 619–633.
33. Uversky, V. N., and Fink, A. L. (2004) Conformational constraints for amyloid fibrillation: The importance of being unfolded. *Biochim. Biophys. Acta 1698*, 131–153.
34. Lindgren, M., Sörgjerd, K., and Hammarström, P. (2005) Detection and characterization of aggregates, prefibrillar amyloidogenic oligomers, and protofibrils using fluorescence spectroscopy. *Biophys. J. 88*, 4200–4212.
35. Uversky, V. N., and Fink, A. L., Eds. (2006) *Protein Misfolding, Aggregation and Conformational Diseases: I. Protein Aggregation and Conformational Disorders*, Springer, New York.
36. Uversky, V. N., and Fink, A. L., Eds. (2007) *Protein Misfolding, Aggregation and Conformational Diseases: II. Molecular Mechanisms of Conformational Diseases*, Springer, New York.
37. Floudas, C. A., Fung, H. K., McAllister, S. R., Mönnigmann, M., and Rajgaria, R. (2006) Advances in protein structure prediction and de novo protein design: A review. *Chem. Eng. Sci. 61*, 966–988.
38. Jones, C. M., Henry, E. R., Hu, Y., Chan, C.-K., Luck, S. D., Bhuyan, A., Roder, H., Hofrichter, J., and Eaton, W. A. (1993) Fast events in protein folding initiated by nanosecond laser photolysis. *Proc. Natl. Acad. Sci. U.S.A. 90*, 11860–11864.
39. Pascher, T., Chesick, J. P., Winkler, J. R., and Gray, H. B. (1996) Protein folding triggered by electron transfer. *Science 271*, 1558–1560.
40. Mines, G. A., Pascher, T., Lee, S. C., Winkler, J. R., and Gray, H. B. (1996) Cytochrome *c* folding triggered by electron transfer. *Chem. Biol. 3*, 491–497.
41. Telford, J. R., Wittung-Stafshede, P., Gray, H. B., and Winkler, J. R. (1998) Protein folding triggered by electron transfer. *Acc. Chem. Res. 31*, 755–763.
42. Chen, E., Wittung-Stafshede, P., and Kliger, D. S. (1999) Far-UV time-resolved circular dichroism detection of electron-transfer-triggered cytochrome *c* folding. *J. Am. Chem. Soc. 121*, 3811–3817.
43. Pascher, T. (2001) Temperature and driving force dependence of the folding rate of reduced horse heart cytochrome *c*. *Biochemistry 40*, 5812–5820.
44. Hagen, S. J., Latypov, R. F., Dolgikh, D. A., and Roder, H. (2002) Rapid intrachain binding of histidine-26 and histidine-33 to heme in unfolded ferrocytochrome *c*. *Biochemistry 41*, 1372–1380.
45. Chen, E., Goldbeck, R. A., and Kliger, D. S. (2003) Earliest events in protein folding: Submicrosecond secondary structure formation in reduced cytochrome *c*. *J. Phys. Chem. A 107*, 8149–8155.
46. Pabit, S. A., Roder, H., and Hagen, S. J. (2004) Internal friction controls the speed of protein folding from a compact configuration. *Biochemistry 43*, 12532–12538.
47. Nishida, S., Nada, T., and Terazima, M. (2004) Kinetics of intermolecular interaction during protein folding of reduced cytochrome *c*. *Biophys. J. 87*, 2663–2675.
48. Kumar, R., Prabhu, N. P., and Bhuyan, A. K. (2005) Ultrafast events in the folding of ferrocytochrome *c*. *Biochemistry 44*, 9359–9367.

49. Dolgikh, D. A., Kolomiets, A. P., Bolotina, I. A., and Ptitsyn, O. B. (1984) 'Molten-globule' state accumulates in carbonic anhydrase folding. *FEBS Lett. 165*, 88–92.
50. Pinheiro, T. J. T., Elöve, G. A., Watts, A., and Roder, H. (1997) Structural and kinetic description of cytochrome *c* unfolding induced by the interaction with lipid vesicles. *Biochemistry 36*, 13122–13132.
51. Davis-Searles, P. R., Morar, A. S., Saunders, A. J., Erie, D. A., and Pielak, G. J. (1998) Sugar-induced molten globule model. *Biochemistry 37*, 17048–17053.
52. Das, T. K., Mazumdar, S., and Mitra, S. (1998) Characterization of a partially unfolded structure of cytochrome *c* induced by sodium dodecyl sulphate and the kinetics of its refolding. *Eur. J. Biochem. 254*, 662–670.
53. Sedlák, E., and Antalík, M. (1999) Molten globule-like state of cytochrome *c* induced by polyanion poly(vinylsulfate) in slightly acidic pH. *Biochim. Biophys. Acta 1434*, 347–355.
54. Sanghera, N., and Pinheiro, T. J. T. (2000) Unfolding and refolding of cytochrome *c* driven by the interaction with lipid micelles. *Protein Sci. 9*, 1194–1202.
55. Hiramatsu, K., and Yang, J. T. (1983) Cooperative binding of hexadecyltrimethylammonium chloride and sodium dodecyl sulfate to cytochrome *c* and the resultant change in protein conformation. *Biochim. Biophys. Acta 743*, 106–114.
56. Takeda, K., Takahashi, K., and Batra, P. P. (1985) Kinetic aspects of the interaction of horse heart cytochrome *c* with sodium dodecyl sulfate. *Arch. Biochem. Biophys. 236*, 411–417.
57. Oellerich, S., Wackerbarth, H., and Hildebrandt, P. (2003) Conformational equilibria and dynamics of cytochrome *c* induced by binding of SDS monomers and micelles. *Eur. Biophys. J. 32*, 599–613.
58. Moosavi-Movahedi, A. A., Chamani, J., Goto, Y., and Hakimelahi, G. H. (2003) Formation of the molten globule-like state of cytochrome *c* induced by *n*-alkyl sulfates at low concentrations. *J. Biochem. 133*, 93–102.
59. Xu, Q., and Keiderling, T. A. (2004) Effect of sodium dodecyl sulfate on folding and thermal stability of acid-denatured cytochrome *c*: A spectroscopic approach. *Protein Sci. 13*, 2949–2959.
60. Gębicka, L., and Gębicki, J. L. (1999) Kinetic studies on the interaction of ferricytochrome *c* with anionic surfactants. *J. Protein Chem. 18*, 165–172.
61. Chattopadhyah, K., and Mazumdar, S. (2003) Stabilization of partially folded states of cytochrome *c* in aqueous surfactant: Effects of ionic and hydrophobic interactions. *Biochemistry 42*, 14606–14613.
62. Xu, Q., and Keiderling, T. A. (2006) Stop-flow kinetics studies of the interaction of surfactant, sodium dodecyl sulfate, with acid-denatured cytochrome *c*. *Proteins: Struct., Funct., Bioinf. 63*, 571–580.
63. Shapiro, D. B., Goldbeck, R. A., Che, D., Esquerra, R. M., Paquette, S. J., and Kliger, D. S. (1995) Nanosecond optical rotatory dispersion spectroscopy: Application to photolyzed hemoglobin-CO kinetics. *Biophys. J. 68*, 326–334.
64. Urry, D. W. (1967) Model systems for interacting heme moieties. I. The heme undecapeptide of cytochrome *c*. *J. Am. Chem. Soc. 89*, 4190–4196.
65. Davies, A. M., Guillemette, J. G., Smith, M., Greenwood, C., Thurgood, A. G. P., Mauk, A. G., and Moore, G. R. (1993) Redesign of the interior hydrophilic region of mitochondrial cytochrome *c* by site-directed mutagenesis. *Biochemistry 32*, 5431–5435.
66. Goto, Y., Calciano, L. J., and Fink, A. L. (1990) Acid-induced folding of proteins. *Proc. Natl. Acad. Sci. U.S.A. 87*, 573–577.
67. Kuwajima, K. (1989) The molten globule state as a clue for understanding the folding and cooperativity of globular-protein structure. *Proteins: Struct., Funct., Genet. 6*, 87–103.
68. Vickery, L., Nozawa, T., and Sauer, K. (1976) Magnetic circular dichroism studies of low-spin cytochromes. Temperature dependence and effects of axial coordination on the spectra of cytochrome *c* and cytochrome b_5. *J. Am. Chem. Soc. 98*, 351–357.
69. O'Connor, D. B., Goldbeck, R. A., Hazzard, J. H., Kliger, D. S., and Cusanovich, M. A. (1993) Time-resolved absorption and magnetic circular dichroism spectroscopy of cytochrome c_3 from *Desulfovibrio*. *Biophys. J. 65*, 1718–1726.
70. Babul, J., and Stellwagen, E. (1971) The existence of heme-protein coordinate-covalent bonds in denatured solvents. *Biopolymers 10*, 2359–2361.
71. Elöve, G. A., Bhuyan, A. K., and Roder, H. (1994) Kinetic mechanism of cytochrome *c* folding: Involvement of the heme and its ligands. *Biochemistry 33*, 6925–6935.
72. Colón, W., Wakem, L. P., Sherman, F., and Roder, H. (1997) Identification of the predominant non-native histidine ligand in unfolded cytochrome *c*. *Biochemistry 36*, 12535–12541.
73. Thomas, Y. G., Goldbeck, R. A., and Kliger, D. S. (2000) Characterization of equilibrium intermediates in denaturant-induced unfolding of ferrous and ferric cytochromes *c* using magnetic circular dichroism, circular dichroism, and optical absorption spectroscopies. *Biopolymers 57*, 29–36.
74. Russell, B. S., Melenkivitz, R., and Bren, K. L. (2000) NMR investigation of ferricytochrome *c* unfolding: Detection of an equilibrium unfolding intermediate and residual structure in the denatured state. *Proc. Natl. Acad. Sci. U.S.A. 97*, 8312–8317.
75. Russell, B. S., and Bren, K. L. (2002) Denaturant dependence of equilibrium unfolding intermediates and denatured state structure of horse ferricytochrome *c*. *J. Biol. Inorg. Chem. 7*, 909–916.
76. Tanford, C. (1970) Protein denaturation. *Adv. Protein Chem. 24*, 1–95.
77. Greene, R. F., and Pace, C. N. (1974) Urea and guanidine hydrochloride denaturation of ribonuclease, lysozyme, α-chymotrypsin, and β-lactoglobulin. *J. Biol. Chem. 249*, 5388–5393.
78. Pace, C. N. (1986) Determination and analysis of urea and guanidine hydrochloride denaturation curves. *Methods Enzymol. 131*, 266–280.
79. Myers, J. K., Pace, C. N., and Scholtz, J. M. (1995) Denaturant m values and heat capacity changes: Relation to changes in accessible surface areas of protein unfolding. *Protein Sci. 4*, 2138–2148.
80. Hagihara, Y., Tan, Y., and Goto, Y. (1994) Comparison of the conformational stability of the molten globule and native states of horse cytochrome *c*. Effects of acetylation, heat, urea and guanidine-hydrochloride. *J. Mol. Biol. 237*, 336–348.
81. Colón, W., and Roder, H. (1996) Kinetic intermediates in the formation of the cytochrome *c* molten globule. *Nat. Struct. Biol. 3*, 1019–1025.
82. Bixler, J., Bakker, G., and McLendon, G. (1992) Electrochemical probes of protein folding. *J. Am. Chem. Soc. 114*, 6938–6939.
83. Santucci, R., Reinhard, H., and Brunori, M. (1988) Direct electrochemistry of the undecapeptide from cytochrome *c* (microperoxidase) at a glassy carbon electrode. *J. Am. Chem. Soc. 110*, 8536–8537.
84. Harbury, H. A., and Loach, P. A. (1959) Linked functions in heme systems: Oxidation-reduction potentials and absorption spectra of a heme peptide obtained upon peptic hydrolysis of cytochrome *c*. *Proc. Natl. Acad. Sci. U.S.A. 45*, 1344–1359.
85. Taniguchi, V. T., Sailasuta-Scott, N., Anson, F. C., and Gray, H. B. (1980) Thermodynamics of metalloprotein electron transfer reactions. *Pure Appl. Chem. 52*, 2275–2281.
86. Matouschek, A., and Fersht, A. R. (1993) Application of physical organic chemistry to engineered mutants of proteins: Hammond postulate behavior in the transition state of protein folding. *Proc. Natl. Acad. Sci. U.S.A. 90*, 7814–7818.
87. Bai, Y. (1999) Kinetic evidence for an on-pathway intermediate in the folding of cytochrome *c*. *Proc. Natl. Acad. Sci. U.S.A. 96*, 477–480.
88. Englander, S. W. (2000) Protein folding intermediates and pathways studied by hydrogen exchange. *Annu. Rev. Biophys. Biomol. Struct. 29*, 213–238.
89. Zhong, S., Rousseau, D. L., and Yeh, S.-R. (2004) Modulation of the folding energy landscape of cytochrome *c* in salt. *J. Am. Chem. Soc. 126*, 13934–13935.
90. Travaglini-Allocatelli, C., Gianni, S., and Brunori, M. (2004) A common folding mechanism in the cytochrome *c* family. *Trends Biochem. Sci. 29*, 535–541.
91. Rao, D. K., Prabhu, N. P., and Bhuyan, A. K. (2006) Extensive misfolding in the refolding reaction of alkaline ferrocytochrome *c*. *Biochemistry 45*, 8393–8401.
92. Ellis, R. J., and Hartl, F. U. (1999) Principles of protein folding in the cellular environment. *Curr. Opin. Struct. Biol. 9*, 102–110.
93. Yon, J. M. (2001) Protein folding: A perspective for biology, medicine and biotechnology. *Braz. J. Med. Biol. Res. 34*, 419–435.

BI702452U